

Plant-crafted starches for bioplastics production



Domenico Sagnelli^a, Kim H. Hebelstrup^b, Eric Leroy^d, Agnès Rolland-Sabaté^d,
Sophie Guilois^d, Jacob J.K. Kirkensgaard^c, Kell Mortensen^c, Denis Lourdin^d,
Andreas Blennow^{a,*}

^a Department of Plant and Environmental Sciences, University of Copenhagen, Thorvaldsensvej 40, 1871 Frederiksberg C, Denmark

^b Department of Molecular Biology and Genetics, University of Aarhus, Forsøgsvej 1, 4200 Slagelse, Denmark

^c Niels Bohr Institute, University of Copenhagen, Universitetsparken 5, 2100 Copenhagen, Denmark

^d UR1268 Biopolymères Interactions Assemblages, INRA, F-44316 Nantes, France

ARTICLE INFO

Article history:

Received 22 February 2016

Received in revised form 27 June 2016

Accepted 10 July 2016

Available online 12 July 2016

Keywords:

Amylose

Bioplastics

Crystallinity

Mechanics

Rheology

Thermoplastic starch

ABSTRACT

Transgenically-produced amylose-only (AO) starch was used to manufacture bioplastic prototypes. Extruded starch samples were tested for crystal residues, elasticity, glass transition temperature, mechanical properties, molecular mass and microstructure. The AO starch granule crystallinity was both of the B- and Vh-type, while the isogenic control starch was mainly A-type. The first of three endothermic transitions was attributed to gelatinization at about 60 °C. The second and third peaks were identified as melting of the starch and amylose-lipid complexes, respectively. After extrusion, the AO samples displayed Vh- and B-type crystalline structures, the B-type polymorph being the dominant one. The AO prototypes demonstrated a 6-fold higher mechanical stress at break and 2.5-fold higher strain at break compared to control starch. Dynamic mechanical analysis showed a significant increase in the storage modulus (E') for AO samples compared to the control. The data support the use of pure starch-based bioplastics devoid of non-polysaccharide fillers.

© 2016 Elsevier Ltd. All rights reserved.

1. Introduction

Starch consists of two major components, amylose and amylopectin, which differ in their degree of branching and molecular size. Amylose is mostly a linear polymer composed of mainly α -(1-4)-linked glucose residues, with a molecular weight (Mw) of approximately 10^5 – 10^6 g mol⁻¹. Amylopectin is a much larger molecule than amylose (Mw = 10^7 – 10^9 g mol⁻¹) and is a more branched polymer with an α -(1-4)-linked D-glucose backbone and approximately 5% α -(1-6)-linked branches (Blennow et al., 2013). At a higher level of organization starch is arranged in different crystalline polymorphs. These are dependent on the botanical origin and type of organ of the plant and are characterized by two main crystalline structures called A-type and B-type (Pérez, Baldwin, & Gallant, 2009). These complexes, if hydrated, can crystallize into different so-called Vh-type polymorphs, which are classified as type I and type II depending on their melting point and structural stability (Goderis, Putseys, Gommès, Bosmans, & Delcour, 2014).

Being one of the most abundant and versatile polysaccharides on earth, starch is a suitable raw material for the production of new environmentally-friendly bioplastics (e.g. Materbi[®], Novamont). Starch is readily transformable using existing technologies and is an abundant and low-cost commodity that can be easily refined. Starch-based plastics can be transformed into edible and compostable products (Ali Shah, Hasan, Hameed, & Ahmed, 2008). Conventional plastic (e.g. polyolefin based plastics), on the other hand, can be a cause of environmental problems related to their low degradability rates. In fact, the degradation of conventional plastic takes place by producing macro- and micro-plastic fragments that persist in both soil and water (Cole, Lindeque, Halsband, & Galloway, 2011). Alternatively, conventional plastic can be mixed with additives that catalyze the degradation of the polymers through light, heat or mechanical stress, leaving pro-degrading additives in the environment but allowing full degradation of the polymer (Ammala et al., 2011). Thermoplastic starch (TPS) is an alternative that can be produced using different existing techniques including casting, thermo-molding, extrusion and injection molding, traditionally used for the processing of synthetic polymers. An interesting advantage of TPS is the modularity of its different properties. For example, the molecular structure (e.g. the molecular size) and amylose/amylopectin ratio influence

* Corresponding author.

E-mail address: abl@plen.ku.dk (A. Blennow).

List of symbols and abbreviations

λ	Wavelength of the incident laser beam
ν_G	Hydrodynamic coefficient
\bar{R}_G	Z-average radius of gyration
\bar{M}_n	Number average molar mass
\bar{M}_w/\bar{M}_n	Dispersity
\bar{M}_w	Weight-average molar mass
AO	Amylose-only
DMTA	Dynamic mechanical thermal analysis
dn/dc	Refractive index increment
DSC	Differential scanning calorimetry
F_c	Cross flow rate
F_{in}	Channel flow in
F_{out}	Channel flow rate
M_i	Molar mass of the i^{st} slice
R_{Gi}	Radius of gyration of the i^{st} slice
R_H	Hydrodynamic radius
RH	Relative humidity
T_g	Glass transition temperature
WAXS	Wide-angle X-ray scattering

the final properties of starch-based bioplastic (Gillgren, Blennow, Pettersson, & Stading, 2011). Also minor differences in the amylose and phosphate contents and chain length distribution of the amylopectin, as well as granular organization, can result in major differences in physical properties. The modification of such structures may also result in the extensive alteration of film functionality as has been demonstrated for transgenic starches (Gillgren et al., 2011). The amylose/amylopectin ratio is an important factor influencing the mechanical properties of such materials, especially since amylose affects the degree of crystallinity and entanglement. Increased amylose content is typically related to an increase in tensile strength and a decrease in strain (Alves, Mali, Beléia, & Grossmann, 2007). Low elasticity can be avoided by including a plasticizer, usually glycerol. This enables the material to endure increased strain but leads to an unavoidable decline in the original strength of the material (Lourdin, Della Valle, & Colonna, 1995; Myllärinen et al., 2002). In addition, high amylopectin content is correlated with higher strain as a result of its structural characteristics e.g. high molecular size (Hulleman, Jannesen, & Feil, 1998).

Commercial starch-based plastics are chemically modified or blended with synthetic polymers, such as polycaprolactone (PCL), to enhance the plastic behavior of these materials (Bastoli, Bellotti, Del Giudice, & Grilli, 1993).

Alternatively, TPS may be improved by other methods, such as the use of genetically modified (GM) organism. Starch-modifying enzymes produced by GM microorganisms can modulate starch structure and functionality, or GM crops can be engineered to produce tailor-made starches directly in their starch-producing organs by coordinated expression of starch-modifying enzymes (Hebelstrup, Sagnelli, & Blennow, 2015).

In the present study, a new plant-crafted starch (engineered and crafted *in planta*) synthesized by an engineered barley-line called amylose-only (AO, Carciofi et al., 2012), composed of 99% of a rather homogeneous amylose-like α -glucan, was used to produce thermoplastic starch-based prototypes. The samples were manufactured by molding and extrusion and finally tested for crystallinity, dynamic mechanical analysis (DMA) and stress and strain at break. The study demonstrates the potential of using GMO plants for the production of new environmentally-friendly polymers as part of a sustainable production of plastics.

2. Materials and methods**2.1. Materials**

The barley starches used in this study were extracted and purified from two barley lines; a control Golden Promise and amylose only a genetically modified (GM) line, which was generated by RNA interference suppressing all three starch branching enzymes in the Golden Promise background. Briefly, the silencing of all three identified genes of the starch branching enzyme family (SBE1, SBE2a and SBE2b) was achieved by using RNAi suppression. Embryos were isolated from juvenile seeds and used for genetic transformation, mediated by *Agrobacterium tumefaciens*. SBE activities were suppressed to below 20% of the control. The full protocol and details on the transgenic lines is given in Carciofi et al. (2012). All chemicals used were provided by Sigma-Aldrich.

2.2. Methods**2.2.1. Water content determination**

The water content of starch granules were determined for each sample using a thermo-balance (TA instruments, New Castle, DE, USA). The instrument was programmed with a ramp of $10^\circ\text{C min}^{-1}$ to 130°C and then an isotherm for 10 min. Water content was calculated based on the weight variation. For the extruded samples the isotherm was increased up to 3 h to achieve a constant weight at the end of the experiment.

2.2.2. Differential scanning calorimetry (DSC)

The melting temperatures of the native starches were determined by differential scanning calorimetry (DSC) using an automated TA Q100 instrument (TA Instruments, New Castle, DE, USA). Experiments were carried out on aliquots of approximately 15 mg starch placed in stainless steel airtight cells. A single scan was run at 3°C min^{-1} from 0 to 150°C . The melting temperature was defined from the endotherm peak value (Garcia et al., 1996).

2.2.3. Sample preparation and melt processing

The formulations used were prepared by mixing the starch with water and/or glycerol using a pestle and mortar. The mixtures were then stored at 4°C for 24 h to achieve equilibrium between the phases. All the blends were prepared taking into account the native water content of the starch, which was measured as described above. The formulations consisted of starch mixed with water alone (30, 40 and 50% water/dry weight, d.w.) and water plus glycerol (30, 40 and 50% water/d.w. and 23% glycerol/d.w.). The formulations were considered as ratios of all three components. For example, the AO5023 had a 50:50 ratio of starch:water. This is an optimal ratio to achieve melting. The starch:glycerol ratio for this sample was 77:23. Two kinds of thermomechanical processes were employed: compression molding and extrusion. Compression molding was performed using a mold with a circular shape (6 cm diameter 0.01 cm height), heated at 130°C and with a pressure of 10 MPa applied for 10 min. All samples were prepared with a density of $1.5\text{ g starch per cm}^3$ (taking into account the volume of the mold). The pressure was released as the mold was cooled to room temperature. The dimensions of the thermo-molded specimens were measured with a micrometer screw gauge (Mitutoyo) and the samples were stored in a desiccator at $57 \pm 2\%$ relative humidity (RH), which was obtained with saturated NaBr salt solution at $20 \pm 3^\circ\text{C}$ (Lourdin et al., 1995), before analysis.

Extrusion was performed with a twin-micro-compounder (HAAKE Minilab II), which allows the simulation of the extrusion process on batches of less than 10 g (Coatvity et al., 2015). This device consisted of a conical twin-screw extrusion chamber and a recirculation channel, which allowed the residence time of the

biopolymer to be controlled (Leroy et al., 2012). Experiments were conducted at a temperature of 105 °C to suppress water evaporation with a screw-speed of 100 rpm. Due to evaporation, samples without glycerol could not be extruded. Three residence times were used (5, 10 and 20 min) producing three different samples (AO5 min, AO10 min, AO20 min). Extruded samples were stored in a desiccator at 57% RH (saturated NaBr salt) and at 20 ± 3 °C before testing. The control starch was extruded at 100 °C and 50 rpm. These conditions were chosen to obtain complete melting of the control starch and to minimize the degree of de-polymerization achieving a specific mixing energy (SME) between 100 and 200 J/g (Della Valle, Boché, Colonna, & Vergnes, 1995). The SME was calculated as described by Leroy et al. (2012):

$$SME = \int_0^t \frac{T2\pi n}{M60} dt$$

where T is the torque signal at mixing time t, n is the screw speed in rpm and M is the loaded mass.

2.2.4. X-ray scattering

Wide-angle X-ray scattering (WAXS) was performed on hydrated samples using the SAXSLab instrument, NBI, University of Copenhagen, equipped with a 100XL + micro-focus sealed X-ray tube (Rigaku) with a 1.54 Å beam. The scattering patterns were recorded with a 2D 300K Pilatus detector from Dectris. The water content of the samples was adjusted by water phase sorption for 10 days in desiccators at a relative humidity of 90% (saturated BaCl₂) for starches and 57% (saturated NaBr) for molded and extruded samples. Hydrated samples were then sealed between thin mica films to prevent evaporation during the X-ray studies.

In situ temperature scans were performed using a temperature-controlled sample stage (Linkam, Tamworth, UK). Samples were heated with a rate of 1 °C min⁻¹ from 40 to 140 °C with scattering patterns recorded every minute. Relative crystal sizes were estimated using the Sherrer equation assuming an unchanged shape factor. Since the peak used to measure crystal growth appears at the same Bragg angle and is measured with the same wavelength, the relative size between the crystal domains is $\frac{\tau_2}{\tau_1} = \frac{\beta_1}{\beta_2}$, where β is the line broadening at half the maximum intensity (FWHM) of the peak in question. No correction was made for instrument resolution effects and thus the derived changes corresponds to the lower boundaries for crystal growth.

Polymorphic types were estimated using a slightly modified version of the peak fitting routine described by Lopez-Rubio, Flanagan, Gilbert, and Gidley (2008). The angular range was adjusted to fit the experimental range and relevant peak information was added for A-, B- and Vh-types based on the crystallographic information available in the work previously mentioned. Gaussian peaks were fitted and combined with the single broad peak due to the amorphous contribution. This routine does not rely on various estimation methods to extract the amorphous contribution before fitting the full data set. From the fits the relative crystallinity, CR, was estimated from the integrated area of all peaks and total integrated area of scattering intensity as $CR = \frac{A_{peaks}}{A_{total}}$.

The percentage of the different polymorphs was estimated as the ratio of the area under the peaks assigned to any specific type to the total peak area of all the fitted Gaussian peaks.

2.2.5. Mechanical properties

Tensile tests were carried out on extruded samples (base = 3.7 mm, height = 40 mm, thickness = 1.3 mm) where the dimensions were given by the rectangular shape of the extruder dye. The specimens were tested with a material-testing machine (MTS, USA) equipped with a 100 N tensile load cell. The distance

between clamps was 20 mm and the crosshead speed was set at 10 mm min⁻¹. The elongation and tensile stress at break were measured at 25 °C. Each analysis was performed at least in triplicate (Lourdin, Bizot, & Colonna, 1997).

2.2.6. Dynamic mechanical analysis

Dynamic mechanical analysis (DMA) was carried out using the DMA Q800 (TA Instruments, New Castle, DE, USA) in tension mode with an amplitude of 0.1% and a frequency of 1 Hz. A standard heating rate of 3 °C min⁻¹ and a ramp from -50 to 120 °C was used. The experiments were carried out on prototypes with a length of 10 mm (Lourdin, Bizot et al., 1997).

2.2.7. Asymmetrical flow field-flow fractionation coupled with multi-angle laser light scattering (A4F-MALLS)

Starches were pretreated with dimethyl sulfoxide and solubilized by microwave heating under pressure, as previously described (Rolland-Sabate, Guilois, Jaillais, & Colonna, 2011). AO samples were dissolved at 10 mg mL⁻¹ in 1 M KOH for 2 h at 4 °C under gentle stirring and then diluted 10-fold with water. Aliquots of 100 μL were injected after filtration through 5 μm Durapore TM membranes (Waters, Bedford, MA, USA) and the solubilization recovery was calculated. The A4F configuration and membrane were the same as previously described (Rolland-Sabate et al., 2011): control starch was eluted with the flow method previously described for starches (Rolland-Sabate et al., 2011) with slight modifications. The cross flow (F_c) was set at 0.84 mL min⁻¹ for the sample introduction and the focusing/relaxation period (ISO-3000SD pump controlled by Chromeleon software version 6.8 SR14, Thermo Scientific). The sample was injected at 0.20 mL min⁻¹ for 300 s. After injection the pump was stopped and the sample was allowed to relax and focus for 60 s. For elution, the detector flow (F_{out}) was set at 0.84 mL min⁻¹ and F_c was decreased from 0.4 to 0.05 mL min⁻¹, for 480 s, then maintained at 0.05 mL min⁻¹ for 600 s and finally held at 0 mL min⁻¹ for 300 s. AO and extruded AO starches were eluted using the following elution steps: F_c was maintained at 0.6 mL min⁻¹ for 300 s, then decreased from 0.6 to 0.05 mL min⁻¹ for 600 s, maintained at 0.05 mL min⁻¹ for 600 s and finally at 0 mL min⁻¹ for 300 s. Elution recovery rates were calculated from the ratio of the mass eluted from the channel and the injected mass (Rolland-Sabate et al., 2011).

M_i and R_{Gi} (molar mass and radius of gyration of the ist slice) respectively were obtained using the Berry extrapolation (with a first order polynomial fit) of the light scattered to zero angle using Astra[®] software (Wyatt Technology Corporation, version 6.1.2.84 for Windows, Rolland-Sabate et al., 2011). Normalization of the photodiodes was achieved using a low molecular mass pullulan standard (P20 – Showadenko) and dn/dc = 0.146 mL g⁻¹ was used. M_n, M_w, dispersity, M_w/M_n and R_G were calculated (Rolland-Sabate et al., 2011). The hydrodynamic radius (R_H) was calculated and a calibration curve established with monodisperse latex spheres 50–500 nm (Duke scientific, Palo Alto, California, USA) (Rolland-Sabate et al., 2011). The v_G and v_H were determined by fitting the log–log plot of R_G and R_H vs the molar mass (obtained at each slice of the elugram).

2.2.8. Scanning electron microscopy

Extruded samples were mounted on aluminum stubs, sputter coated with gold–palladium and observed at 10 kV in a Quanta 200 SEM instrument (FEI Company, Eindhoven, The Netherlands) (Shaik et al., 2016).

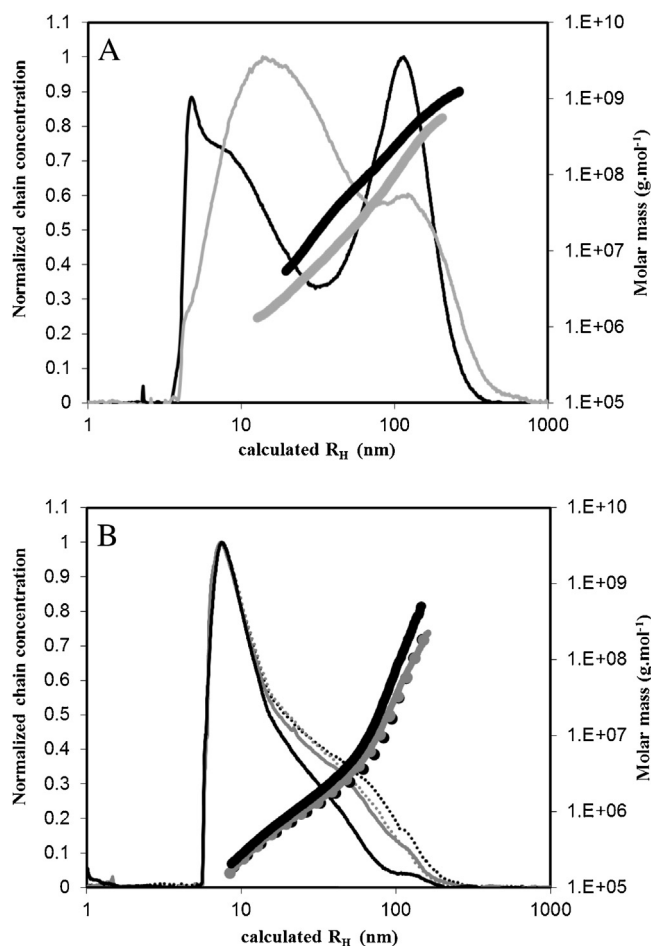


Fig. 1. R_H (thin lines) and molar mass distributions (bold lines) of native and extruded samples. A) control (black) and extruded control starch (grey), B) AO (black, solid line) and extruded AO5 min (black dotted line), AO10 min (grey solid line), AO20 min (grey, dotted line) starches.

3. Results and discussion

3.1. Macromolecular structure, crystallinity, melting and phase transitions of starch granules

An overview of the intrinsic characteristics of the native AO and control starches was established by analyzing their molar mass, crystallinity and melting behavior. For molecular size and molar mass distributions, the starches were dissolved and analyzed by asymmetrical flow field-flow fractionation coupled with multi-angle laser light scattering (AF4-MALLS). The solubilization recoveries were higher than 92% for all samples and the elution recoveries were all higher than 90%, providing representative data for the samples. The size distribution of the native control starch exhibited two populations corresponding to amylose (R_H 6–35 nm) and amylopectin (R_H 30–390 nm, Fig. 1) (Rolland-Sabate et al., 2011). The \bar{M}_w of AO being $9.1 \times 10^6 \text{ g mol}^{-1}$ was about 24-times lower than the control and exhibited a lower \bar{R}_G (199 nm) and a lower dispersity ($\bar{M}_w/\bar{M}_n = 26$, Table 1), as is expected for an AO starch. However, these values were high compared to typical pure amylose samples, but were in line with the presence of large particles, which could be residual branched macromolecules or aggregates (Rolland-Sabate et al., 2011).

ν_G and ν_H , the slopes of the log–log plot of \bar{R}_G and R_H versus molar mass, respectively, provide valuable information on the macromolecular conformation. ν_G and ν_H were around 0.41 for the control, which corresponds to the typical value obtained for a

Table 1

Macromolecular characteristics of samples determined by AF4-MALLS^{a,b}. Weight average molar mass (\bar{M}_w), z-average radius of gyration (\bar{R}_{Gz}), dispersity (\bar{M}_w/\bar{M}_n) and hydrodynamic coefficient (ν_G), specific mixing energy during the extrusion (SME).

	$\bar{M}_w \cdot 10^{-6} \text{ (g mol}^{-1}\text{)}$	$\bar{R}_{Gz} \text{ (nm)}$	\bar{M}_w/\bar{M}_n	SME (J/g)
Control	215.3	251	82	
Extruded control	106.7	241	42	130
AO	9.1	199	26	
AO5 min	8.8	176	27	40
AO10 min	7.0	175	19	277
AO20 min	6.3	181	18	421

^a Values corresponding to the whole peak and obtained by fitting the molar mass and the radius of gyration along the distributions.

^b The experimental uncertainties were 5%.

spheroidal branched macromolecule such as amylopectin (Rolland-Sabate et al., 2011). For AO starch, ν_G values were around 0.35 for molar masses $>10^6 \text{ g mol}^{-1}$ and ν_H values were about 0.6 for molar masses $<10^6 \text{ g mol}^{-1}$ and 0.20 for molar masses $>10^6 \text{ g mol}^{-1}$. The ν_H value of 0.6 corresponds to the theoretical value for a random coil in an optimal solvent, which is in line with the conformation of single amylose chains. This confirms that the major peak (R_H 5–20 nm) corresponds to single amylose chains. The values of 0.2–0.35 account for a very dense structure and were not in agreement with the value expected for amylose in a coiled conformation. The population with molar masses $>10^6 \text{ g mol}^{-1}$ (minor peak, R_H 20–200 nm) therefore most probably consisted of self-aggregated amylose chains in the AF4 channel.

For crystal structure and crystallinity of the native starches, Wide-Angle X-ray Scattering (WAXS) analysis was performed using fully hydrated starch granule samples. The control barley starch had a mixture of 75% A-type and 25% Vh-type crystals, which is a typical diffraction pattern found in normal starch (Yangcheng, Gong, Zhang, & Jane 2016). On the contrary, the AO starch showed a mixed pattern of 68% B-type and 32% Vh-type (Table 2, Supplementary Fig. 1), which is a unique diffraction pattern profile provided by this GMO starch.

The melting behavior of the AO starch was tested using differential scanning calorimetry (DSC) at different concentrations and ratios of water and glycerol as plasticizers. Melting transitions of AO granules were recorded as suspensions containing water alone (AO30, AO40 and AO50, where the numbers denote % water/d.w.) and water plus glycerol (AO3023, AO4023 and AO5023, where the numbers denote % water/d.w. and % glycerol/d.w.) as plasticizers. For the water-only samples, three distinct endothermic peaks were detected (Fig. 2). The first transition was found in the temperature range 60–70 °C and was detected for samples hydrated with 40% and 50% water. This transition had an enthalpy dependent on the water content and corresponding to starch gelatinization (Colonna & Mercier, 1985; Källman et al., 2015), which is the process of disorganization of the native semi-crystalline structure of the starch granules. The main endothermic peak had an onset temperature (T_0) in the range 80–105 °C, which increased with decreasing water content. This transition is termed the “M” transition. This transition is not related to gelatinization, but represents the melting of starch crystallites (Biliaderis, 2009, Chapter 8). For starch-containing native lipids, an endothermic transition is usually detected around 130 °C (Jovanovich & Anon, 1999; Marinopoulou, Papastergiadis, Raphaelides, & Kontominas, 2016) which is the melting of amylose/lipid complexes that are formed at temperatures just above the melting point of starch (Fig. 2).

In the presence of glycerol the third endothermic peak was absent (Fig. 2). Glycerol has been shown to affect the interaction of wheat amylose with native lipids by increasing the temperature of dissociation of the complexes (Jovanovich & Anon, 1999). We propose that this effect is related to the interaction of glycerol

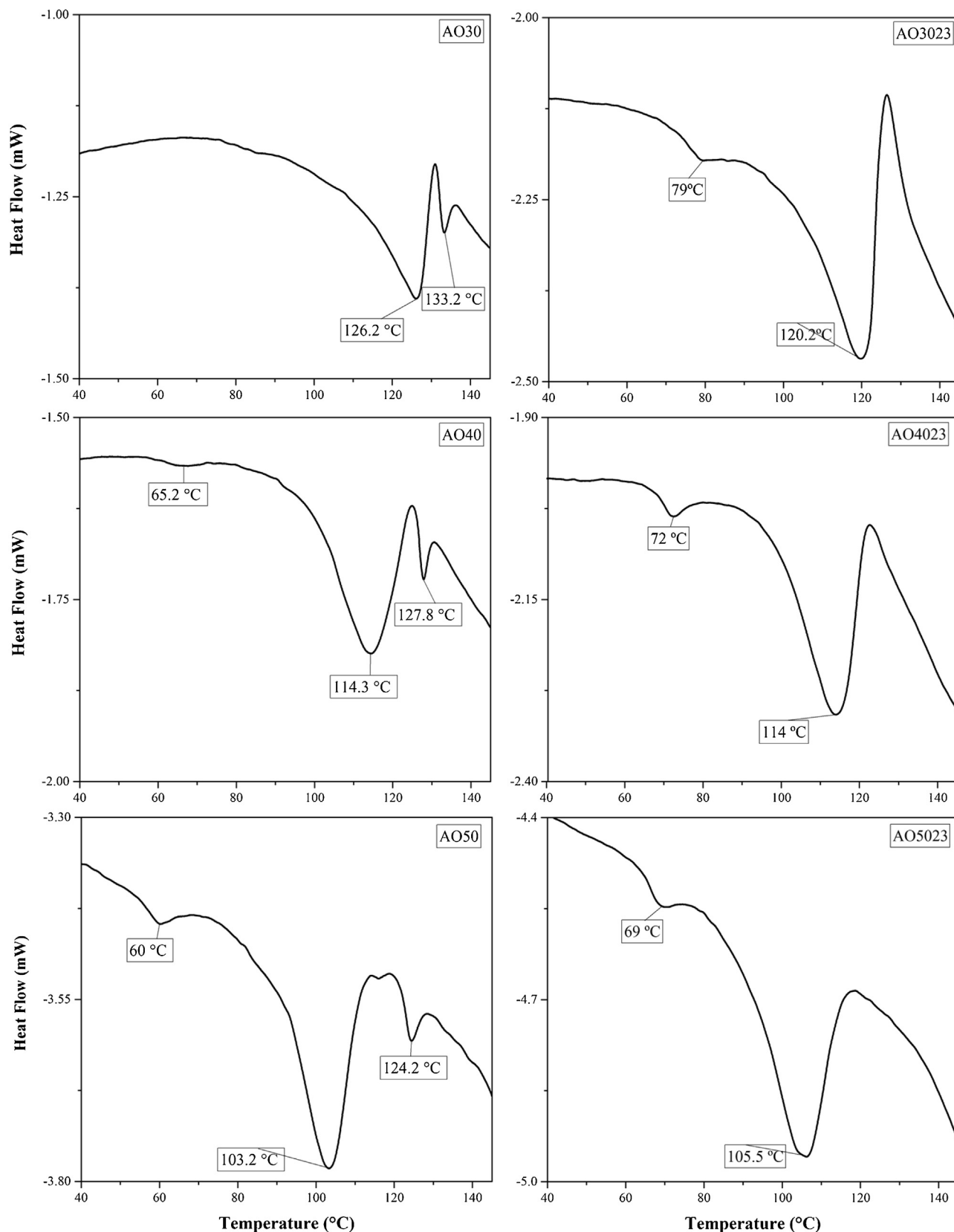


Fig. 2. DSC thermograms showing the effect of glycerol on the thermal phase transition behavior of AO as a function of water \pm glycerol content. Water-only systems: AO30, AO40 and AO50; water plus glycerol systems: AO3023, AO4023 and AO5023, as described in the text.

with free amylose chains and un-melted amylose/lipid complexes keeping them in a disordered state. The control starch, which contained 25% water, had a melting temperature of 120 °C (results not

shown). The endothermic profile of control starch transitions was in accordance with previously published data showing the melting of both amylopectin and amylose/lipid complexes (Biliaderis, 2009,

Table 2
Crystallinity (%) and relative size of the crystals.

	A-type (%)	B-type (%)	Vh-type (%)	Relative crystallinity	Vh - total	Relative size
Native starches						
Control	75	0	25	21	5	nd
AO	0	69	32	24	8	1
Molded TPS						
AO30; AO3023	0	72; 76	28; 24	25; 24	7; 6	3; 4
AO40; AO4023	0	76; 80	24; 20	24; 21	6; 4	2; 4
AO50; AO5023	0	78; 84	22; 16	23; 20	5; 3	1; 2
Extruded TPS						
AO5 min	0	85	15	32	5	2
AO10 min	0	81	19	32	6	4
AO20 min	0	84	16	34	5	4
Control	0	84	16	27	4	nd

nd: not determined.

Chapter 8; Colonna & Mercier, 1985; Song & Jane, 2000; Yoshimoto, Tashiro, Takenouchi, & Takeda, 2000; Källman et al., 2015).

Dynamic WAXS analysis was also performed at increasing temperatures to test if the effect of glycerol observed in the DSC data could be explained by inhibition of recrystallization. The samples with 50% water \pm glycerol were chosen since these gave

well-defined transition profiles. For the samples without glycerol, recrystallization of the starch was induced at temperature above the melting point (Fig. 3). This result is in agreement with previously published data (Le Bail et al., 1999) on normal and high amylose starches and is confirmed in this study for a natural 99% amylose transgenic system. Interestingly, the diffractogram

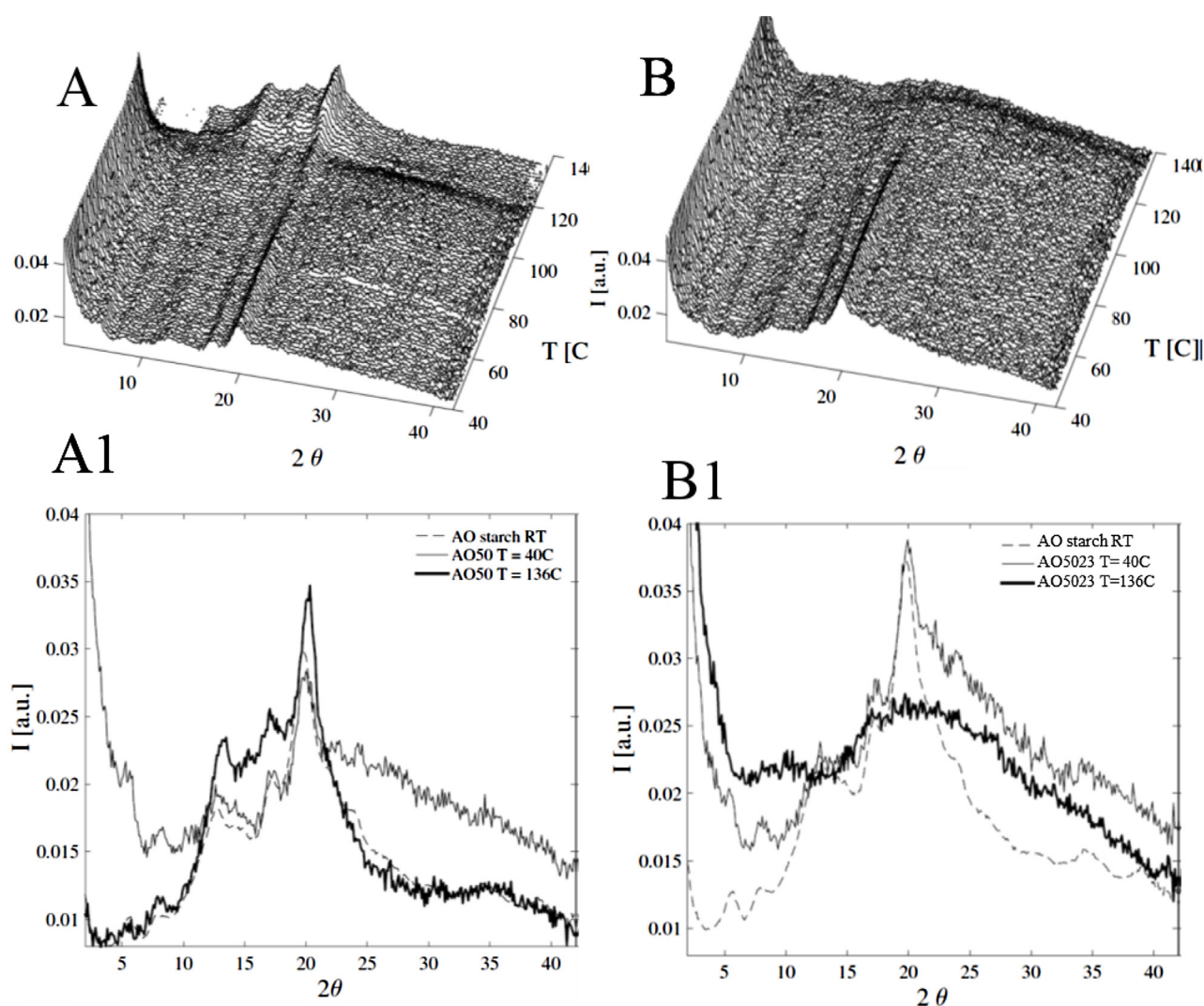


Fig. 3. X-ray monitoring of the melting of amylose-only starch with 50% water and 50% water/23% glycerol as indicated: (A) Diffraction diagram of AO50 recorded at 3°C min^{-1} , (A1) Overlay of AO50 diffraction diagram at $T = 40^\circ\text{C}$, $T = 136^\circ\text{C}$ and $T = 25^\circ\text{C}$. (B) Diffraction diagram of AO5023 recorded at 3°C min^{-1} , (B1) Overlay of AO5023 diffraction diagram at $T = 40^\circ\text{C}$, $T = 136^\circ\text{C}$ and $T = 25^\circ\text{C}$.

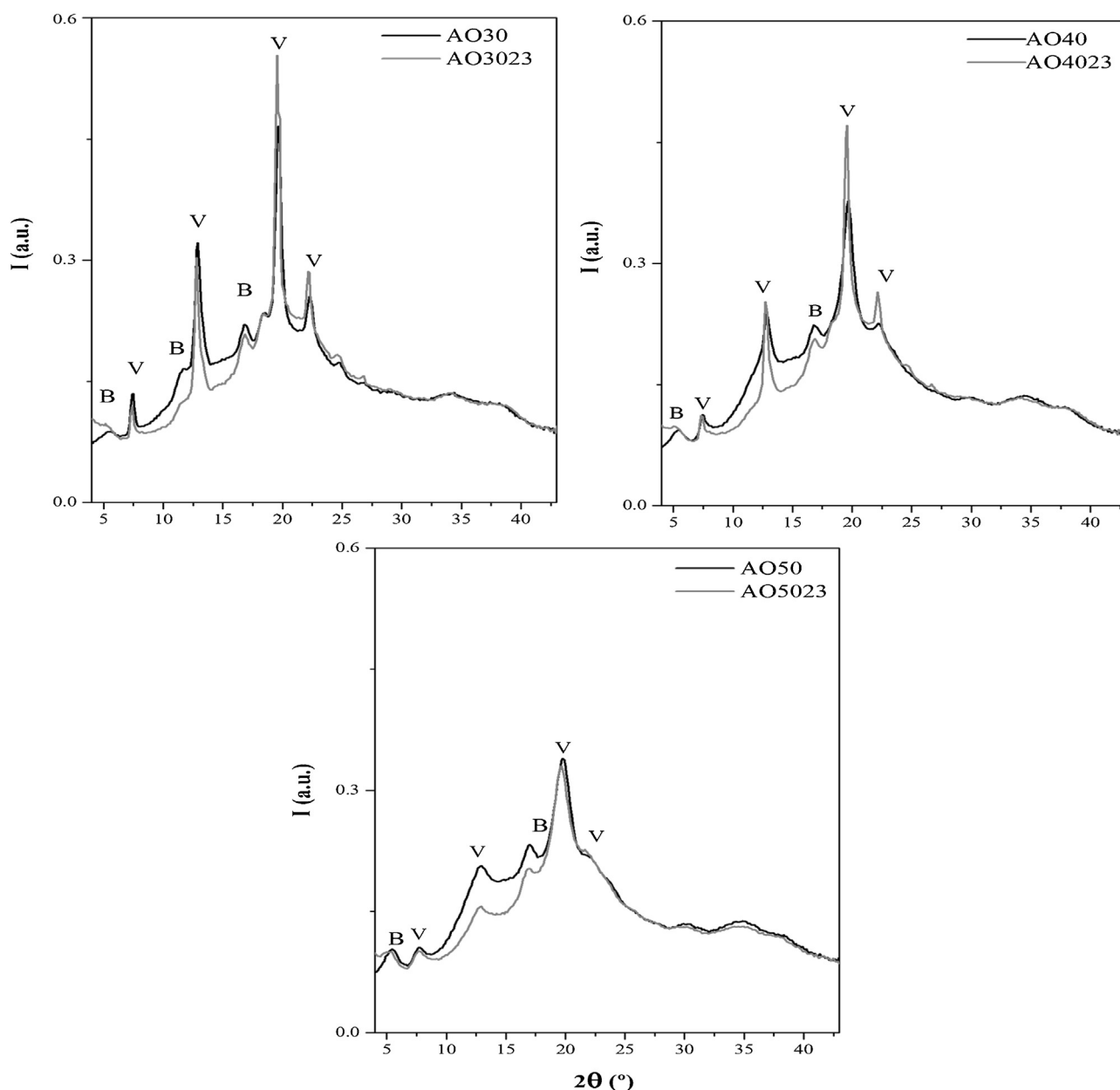


Fig. 4. Diffractograms of thermo-molded samples demonstrating the effect of different water and glycerol contents on crystal formation: (A) Overlay of AO30 and AO3023; (B) Overlay of AO40 and AO4023; (C) Overlay of AO50 and AO5023.

of the glycerol-containing samples showed different behavior. For these samples the melting temperature of starch crystallites was increased by approximately 15 °C and the recrystallization observed in the samples without glycerol was absent (Fig. 3). This is the first time that such an effect has been observed as a function of glycerol content for native starch granules. However, similar effects have been demonstrated for starch systems with excess water (Le Bail et al., 1999). These data confirm the DSC data above and suggest that glycerol prevents the formation of the specific crystalline complexes that were present in starch samples with water but no glycerol. The prevention of the recrystallization can possibly be considered as an effect of the interaction of glycerol with amylose and/or amylose/lipid complexes (Fig. 3). The high hygroscopicity of glycerol can retain water in the system, avoiding water re-localization and amylose nucleation.

3.2. Crystallinity and crystalline polymorphs of thermo-molded and extruded samples

The melting processing of the sample (either by compression molding or extrusion), followed by storage at 57% RH, resulted in significant modification of the crystallinity of all formulations as determined by WAXS. Total crystallinity was not significantly changed for AO compression molded samples, however, for extruded samples higher crystallinity was observed. The relative contribution of B-type and Vh-type crystalline structures was also altered by processing, with an increase of the B-type content and corresponding decrease of Vh-type in all samples. For the control starch, which had A-type and Vh-type native crystallinity, the extruded sample only displayed B-type and Vh-type. This indicates complete melting of the initial A-type crystalline phase during processing, as has been previously suggested (Van Soest, Hulleman,

De Wit, & Vliegenthart, 1996), followed by recrystallization during storage at 57% RH. For the AO samples, the increase in B-type content indicates that such recrystallization also takes place. However, the extent of transformation of the native B-type crystallinity is unknown.

For the compression-molded samples, both water and glycerol were found to have an effect. In particular, the diffraction peaks were less sharp with increasing amount of water indicating a decrease in the dimensions of the crystals and relative crystallinity. However, an increase in B-type crystallinity was found, which is in agreement with a previous study on glycerol-plasticized potato starch (Hulleman, Kalisvaart, Janssen, Feil, & Vliegenthart, 1999). Samples prepared in the presence of glycerol showed a decreased amorphous phase suggesting that after cooling the glycerol supported crystal growth (Fig. 4). The presence of glycerol slightly increased the sharpness of the peaks indicating increased crystal size (Fig. 4, Table 2).

The low melting temperature and low crystallinity of the high-water content samples, demonstrated above, suggests that 50% water content should be used for extrusion (50% water and 23% glycerol) to generate optimally plasticized prototypes. The A-type crystals in the control were completely melted by the extrusion process and subsequently recrystallized to form Vh- and B-type crystals (Supplementary Fig. 1). The hydrated native AO starch had 69% B-type crystallinity and 32% Vh-type and showed a similar pattern after extrusion, with only a slightly higher amount of B-type (85%) crystals (Table 2). There was a tendency for the formation of B-type at the expense of Vh-type crystals in both extruded and molded samples compared to the native starches and water-only samples. Interestingly, the control starch showed a similar tendency i.e. converting initial A-type crystals into mainly B- and Vh-types with the same ratio as the extruded and molded AO starch.

The data also revealed a trend related to the processing time (5, 10 or 20 min melting in the extruder). Increasing the cycling time increased crystal growth during the storage period at the expense of amorphous material as is indicated by the sharpening of the diffraction signals with residence time (Supplement Fig. 1, Table 2). This result is in agreement with a previous study (Van Soest et al.,

1996), which demonstrated a positive correlation with residence time during extrusion and crystallinity.

3.3. Mechanical properties

The extruded specimens (AO at 5, 10 and 20 min melting) were evaluated by tensile tests in order to characterize their stress and strain behavior. The samples fabricated from the AO starch melted for 5 min in the extruder showed the highest mechanical values. A decrease in performance was observed the longer the residence time in the extruder (10 and 20 min).

For the AO5 min sample a 6-fold higher tensile stress at break (σ_R) (AO = 7.3 ± 0.1 , control = 1.4 ± 0.3) and 2-fold higher elongation at break (ϵ_r) (AO = $160\% \pm 7$, control = $94\% \pm 0.7$) were observed compared to the control barley starch extrudates (Fig. 5). This demonstrates a noteworthy stabilizing effect of amylose for both mechanical parameters. Interestingly, these data were in agreement with collected mechanical data for starch-based materials (Follain, Joly, Dole, & Bliard, 2005) and confirm that the performance of the AO materials differ from other typical amylose prototypes, including ones with 30% glycerol. For example, the AO5 min had an elongation at break (ϵ_r) that was 7–16 fold higher than wheat high-amylose starch (70–100%) extruded with 22–30% glycerol ($\epsilon_r = 10$ –25%). However, the tensile stress at break (σ_R) for the AO samples was lower than for the pure wheat amylose with 22% glycerol ($\sigma_R = 20$ MPa), but similar to the wheat-amylose mixed with 30% glycerol ($\sigma_R \sim 8$ MPa) (Follain et al., 2005). Increasing the melting time inside the bench top extruder, which varied from 5 to 20 min, significantly decreased the elongation at break for the AO samples (Fig. 4). The decrease in mechanical performance, as demonstrated by a decreased Young's moduli (E) (Supplementary Table 1), for the samples with long residence times in the extruder (Fig. 4) is possibly due to the effect of chain scission of the starch during the melting process. This was further investigated by AF4-MALLS, see below. The size of the crystals (Table 2) was a negative factor for the mechanical properties and demonstrated that large crystals decreased the ductility and toughness of the samples.

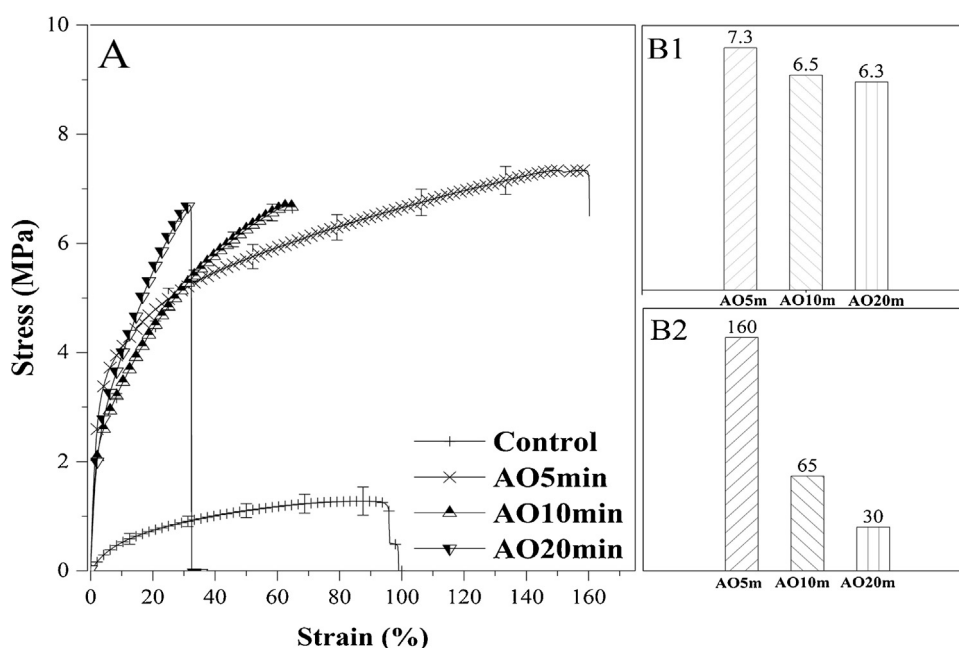


Fig. 5. Mechanical properties of extruded samples. (A) Stress and strain overlay of extruded samples with the control; (B1) Stress at break (MPa) and (B2) Elongation at break (%) of prototypes.

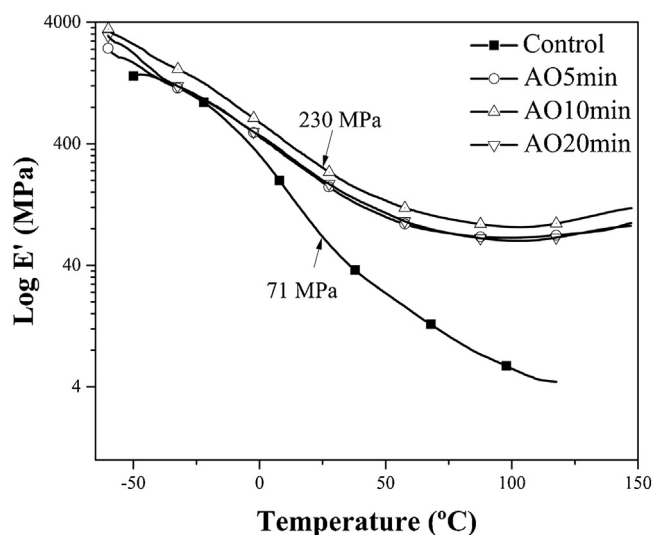


Fig. 6. Storage moduli of all extrudate samples measured by DMA showing the effect of amylose on the increase in the stored energy compared to control starch (The E' value shown is calculated at $T = 25^\circ\text{C}$).

3.4. Dynamic visco-elastic properties

The samples extruded at 5, 10 and 20 min recycling time were analyzed for their visco-elastic properties using a dynamic mechanical analyzer (DMA). Storage (E') and loss moduli (E'') were measured using the DMA in tension mode and by applying a scanning temperature protocol. This experimental set up permitted extraction of the mechanical relaxation region by identifying the peak in the $\tan \delta$, which is associated with the α -peak of the glass transition.

All the AO samples showed similar transitions and a wide mechanical relaxation region (Supplementary Fig. 2). The $\tan \alpha$ -peak, which corresponds to T_g , was around $25 \pm 2^\circ\text{C}$ for all samples. A second peak appeared at about 100°C . The origin of this peak is still unclear, but it could be due to dehydration of the sample during

the heating scan. A very high storage modulus (230 ± 20 MPa) and a rubbery plateau were detected at 25°C for the AO samples (Fig. 6). In comparison, the modulus of the control sample was about 4-times lower (71 ± 10 MPa), which is due to the different amounts of amylose in the samples. Even small differences in the amylose content can affect specific rheological and mechanical properties (Byars & Singh, 2016; Follain et al., 2005; Freitas, Paula, Feitosa, Rocha, & Sierakowski, 2004) and our data demonstrates major changes corresponding to large differences in amylose content.

A relationship between the percentage of Vh- and B-type crystals and the storage modulus was observed only for the AO system where the storage modulus had a tendency to increase with the amount of Vh-type crystals in the sample. The crystal size (Table 2) was also found to be related to the glass relaxation temperature (Supplementary Table 2), as calculated from DMA data. The loss modulus at 25°C was found to be dependent on the recycling time inside the extruder. Particularly, increasing the recycling time increased the loss modulus (AO5 min = 116 MPa, AO10 min = 137 MPa, AO20 min = 211 MPa). In comparison with the control (30 MPa) the AO samples had higher loss moduli.

3.5. Macromolecular structure of extruded samples

Following extrusion, the size distribution of amylopectin, determined by AF4-MALLS, decreased and a large peak appeared at R_H ranging from 5 to 75 nm. This peak corresponds to the amylose and branched products resulting from the degradation of amylopectin during extrusion (Fig. 1A). The \bar{M}_w values were $2.15 \times 10^8 \text{ g mol}^{-1}$ and $1.06 \times 10^8 \text{ g mol}^{-1}$ and the \bar{R}_G values were 241 nm and 251 nm for control and extruded control starches, respectively (Table 1). The \bar{R}_G and molar mass of the control starch decreased after extrusion, whereas the dispersity increased 1.9-fold. This evolution of molar mass distributions after extrusion was in agreement with a previous study (Sankri et al., 2010).

Compared to the control samples, AO starch and AO extrudates exhibited completely different size distributions. A large peak was obtained in the AF4-MALLS elugram corresponding to amylose (R_H 5–20 nm) and a second minor peak (R_H 20–200 nm) correspond-

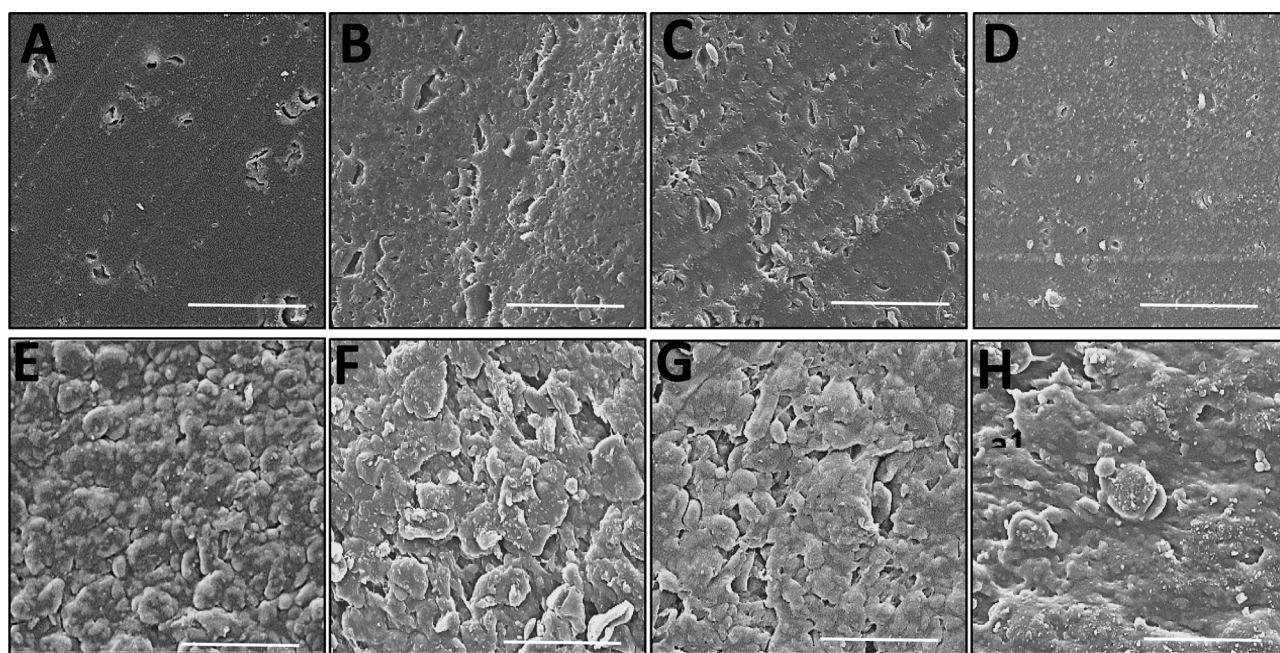


Fig. 7. SEM micrographs of cross-sectional and external surfaces of extruded starches. Cross sections: (A) AO5 min (B) AO10 min (C) AO20 min (D) control. External surfaces (E) AO5 min, (F) AO10 min, (G) AO20 min (H) control. Scale bars show $50 \mu\text{m}$.

ing to larger molecules (Fig. 1B). After extrusion, \bar{M}_w and \bar{M}_w/\bar{M}_n decreased from $8.8 \times 10^6 \text{ g mol}^{-1}$ to $6.3 \times 10^6 \text{ g mol}^{-1}$ and from 27 to 18 nm, respectively, with increased extrusion time (Table 1). This slight decrease in macromolecular size is most probably related to minor depolymerization occurring during extrusion. The sensitivity of such extrusion-based chain scission was clearly lower for AO starch compared to the control starch. For extruded control samples v_G and v_H after extrusion were unchanged, suggesting that the spherical conformation remained. For the AO extruded samples, v_G and v_H values confirmed the single amylose chain conformation. Importantly, the decrease in mechanical performance for the samples with longer residence times in the extruder, observed in the mechanical tests shown above (Fig. 5), is confirmed by the decrease in molar mass. Especially for the AO samples, strain increased with the molar mass of the amylose. Using both natural and artificial amylose:amylopectin mixtures (Lourdin et al., 1995) such relationships have been found for molar mass, amount of amylose and mechanical strength (Lourdin et al., 1995). Our data confirms that the molar mass of a natural amylose-like α -glucan affects the elongation of extruded specimens.

3.6. Extrudate specimen surface microstructure

Surface microstructure of the extruded prototypes, as analyzed by scanning electron microscopy (SEM), showed rough external textures for all the specimens prepared from the AO starch. This revealed that the granular structures at the surface were not completely melted (Fig. 7). However, the control starch sample showed a relatively smooth surface. Inspection of cross sections revealed that the melting of the starch was more homogenous for all specimens. Still, the AO5 min and the control specimens showed relatively smoother cross-sectional surfaces compared to the A10 min and A20 min samples. All specimens exhibited pores (Fig. 7), which were probably produced by water vapor cavities formed during the extrusion.

4. Conclusions

Starch-based bioplastic prototypes fabricated from an almost amylopectin-free starch synthesized directly in the barley grain behaved differently compared to most high-amylose systems analyzed to date. Melting conditions for subsequent extrusion cooking was determined from initial DSC and X-ray scattering data. These data demonstrated effects related to interaction between the glycerol and amylose during the heating process. A subsequent thermo-molding screen provided optimized formulations and thermal protocols for extrusion. The finally extruded AO starch prototypes had mechanical performances characterized by elevated stress and strain at break compared to a control starch. The AO prototypes had storage moduli comparable to control starch prototypes, as shown by DMA data. The formulation and processing conditions influenced the characteristics of the samples produced in terms of molar mass distribution, residual crystallinity and mechanical properties. The data support the use of pure starch-based bioplastics devoid of non-polysaccharide fillers.

Acknowledgements

We would like to thank Lun Li Krusholt for help with the extraction of the starch and Michelle Derbyshire of MD Writing Services, for providing assistance with the preparation of this manuscript. We would also like to thank the Center for Advanced Bioimaging, Faculty of Science, University of Copenhagen for use of their microscopy facilities. This work was funded by The Danish Council

for Independent Research Technology and Production Sciences and Carlsberg Foundation.

Appendix A. Supplementary data

Supplementary data associated with this article can be found in the online version, at <http://dx.doi.org/10.1016/j.carbpol.2016.07.039>.

References

- Ali Shah, A., Hasan, F., Hameed, F., & Ahmed, S. (2008). Biological degradation of plastics: A comprehensive review. *Biotechnology Advance*, 26, 246–265.
- Alves, V. D., Mali, S., Beléia, A., & Grossmann, M. V. E. (2007). Effect of glycerol and amylose enrichment on cassava starch film properties. *Journal of Food Engineering*, 78, 941–946.
- Ammala, A., Bateman, S., Dean, K., Petinakis, E., Sangwan, P., Wong, S., et al. (2011). An overview of degradable and biodegradable polyolefins. *Progress Polymer in Science*, 36, 1015–1049.
- Bastoli, C., Bellotti, V., Del Giudice, L., & Grilli, G. (1993). Mater-bi: Properties and biodegradability. *Journal of Polymers and the Environment*, 1, 181–191.
- Biliaderis, C. G. (2009). Structural transitions and related physical properties of starch. In *Starch* (3rd ed.). Elsevier.
- Blennow, A., Jensen, S. L., Shaik, S. S., Skryhan, K., Carciofi, M., Holm, P. B., et al. (2013). Future cereal starch bioengineering: Cereal ancestors encounter gene technology and designer enzymes. *Cereal Chemistry*, 90, 274–287.
- Byars, J. A., & Singh, M. (2016). Rheological and textural properties of pulse starch gels. *Starch/Stärke*, 68, 1–7.
- Carciofi, M., Blennow, A., Jensen, S. L., Shaik, S. S., Henriksen, A., Buléon, A., et al. (2012). Concerted suppression of all starch branching enzyme genes in barley produces amylose-only starch granules. *BMC Plant Biology*, 12, 223.
- Coatv, G., Gautier, N., Pontoire, B., Buléon, A., Lourdin, D., & Leroy, E. (2015). Shape memory starch-clay bionanocomposites. *Carbohydrate Polymers*, 116, 307–313.
- Cole, M., Lindeque, P., Halsband, C., & Galloway, S. T. (2011). Microplastics as contaminants in the marine environment: A review. *Marine Pollution Bulletin*, 62, 2588–2597.
- Colonna, P., & Mercier, C. (1985). Gelatinization and melting of maize and pea starches with normal and high-amylose genotypes. *Phytochemistry*, 24, 1667–1674.
- Della Valle, G., Boché, Y., Colonna, P., & Vergnes, B. (1995). The extrusion behaviour of potato starch. *Carbohydrate Polymers*, 28(3), 255–264.
- Follain, N., Joly, C., Dole, P., & Bliard, C. (2005). Mechanical properties of starch-based materials. I. Short review and complementary experimental analysis. *Journal of Applied Polymer Science*, 97, 1783–1794.
- Freitas, R. A., Paula, R. C., Feitosa, J. P. A., Rocha, S., & Sierakowski, M. R. (2004). Amylose contents, rheological properties and gelatinization kinetics of yam (*Dioscorea alata*) and cassava (*Manihot utilisima*) starches. *Carbohydrate Polymers*, 55(1), 3–8.
- Garcia, V., Colonna, P., Lourdin, D., Buleon, A., Bizot, H., & Ollivon, M. (1996). Thermal transitions of cassava starch at intermediate water contents. *Journal of Thermal Analysis*, 47(5), 1213–1228.
- Gillgren, T., Blennow, A., Pettersson, A. J., & Stading, M. (2011). Modulating rheo-kinetics of native starch films towards improved wet-strength. *Carbohydrate Polymers*, 83, 383–391.
- Goderis, B., Putseys, J. A., Gommers, C. J., Bosmans, G. M., & Delcour, J. M. (2014). The structure and thermal stability of amylose-lipid complexes: A case study on amylose. *Crystal Growth and Design*, 14(7), 3221–3233.
- Hebelstrup, K. H., Sagnelli, D., & Blennow, A. (2015). The future of starch bioengineering: GM microorganisms or GM plants? *Frontiers in Plant Science*, 6, 247.
- Hulleman, S. H. D., Janssen, F. H. P., & Feil, H. (1998). The role of water during plasticization of native starches. *Polymer*, 39, 2043–2048.
- Hulleman, S. H. D., Kalisvaart, M. G., Janssen, F. H. P., Feil, H., & Vliegthart, J. F. G. (1999). Origins of B-type crystallinity in glycerol-plasticized, compression-moulded potato starches. *Carbohydrate Polymers*, 39(4), 351–360.
- Jovanovich, G., & Anon, M. C. (1999). Amylose-lipid complex, physicochemical properties and the effects of different variables. *LWT—Food Science and Technology*, 32, 95–101.
- Källman, A., Vamadevan, V. M., Bertoft, E., Koch, K., Seetharaman, K., Aman, P., et al. (2015). Thermal properties of barley starch and its relation to starch characteristics. *International Journal of Biological Macromolecules*, 81, 692–700.
- Le Bail, P., Bizot, H., Ollivon, M., Keller, G., Bourgaux, C., & Buléon, A. (1999). Monitoring the crystallization of amylose-lipid complexes during maize starch melting by synchrotron x-ray diffraction. *Biopolymers*, 50, 99–110.
- Leroy, E., Jacquet, P., Coatv, G., Reguerre, A. L., & Lourdin, D. (2012). Compatibilization of starch-zein melt processed blends by an ionic liquid used as plasticizer. *Carbohydrate Polymers*, 89, 3.
- Lourdin, D., Della Valle, G., & Colonna, P. (1995). Influence of amylose content on starch films and foams. *Carbohydrate Polymers*, 27, 261–270.
- Lourdin, D., Bizot, H., & Colonna, P. (1997). 'Antiplasticization' in starch-Glycerol films? *Journal of Applied Polymer Science*, 63, 1047–1053.

- Lopez-Rubio, A., Flanagan, B. M., Gilbert, E. P., & Gidley, M. J. (2008). A novel approach for calculating starch crystallinity and its correlation with double helix content: A combined XRD and NMR study. *Biopolymers*, *89*(9), 1097–10282.
- Marinopoulou, A., Papastergiadis, E., Raphaelides, S. N., & Kontominas, M. G. (2016). Morphological characteristics, oxidative stability and enzymic hydrolysis of amylose–fatty acid complexes. *Carbohydrate Polymers*, *141*, 106–115.
- Myllärinen, P., Partanen, R., Seppälä, J., & Forssell, P. (2002). Effect of glycerol on behaviour of amylose and amylopectin films. *Carbohydrate Polymers*, *50*, 355–361.
- Pérez, S., Baldwin, P. M., & Gallant, D. J. (2009). Structural features of starch granules I. In *Starch* (3rd ed.). Elsevier.
- Rolland-Sabate, A., Guilois, S., Jaillais, B., & Colonna, P. (2011). Molecular size and mass distributions of native starches using complementary separation methods: Asymmetrical flow field flow fractionation (A4F) and hydrodynamic and high performance size exclusion chromatography (HDC-HPSEC). *Analytical and Bioanalytical Chemistry*, *399*, 1493–1505.
- Sankri, A., Arhaliass, A., Dez, I., Gaumont, A. C., Grohens, Y., Lourdin, D., et al. (2010). Thermoplastic starch plasticized by an ionic liquid. *Carbohydrate Polymers*, *82*, 256–263.
- Shaik, S. S., Obata, T., Hebelstrup, H. K., Schwanh, K., Fernie, R. A., Mateiu, V. R., et al. (2016). Starch granule re-structuring by starch branching enzyme and glucan water dikinase modulation affects caryopsis physiology and metabolism. *Public Library of Science*, *11*, 2.
- Song, Y., & Jane, J. (2000). Characterization of barley starches of waxy, normal, and high amylose varieties. *Carbohydrate Polymers*, *41*(4), 365–377.
- Van Soest, J. J. G., Hulleman, S. H. D., De Wit, D., & Vliegenthart, J. F. G. (1996). Crystallinity in starch bioplastics. *Industrial Crops and Products*, *5*, 11–22.
- Yangcheng, H., Gong, L., Zhang, Y., & Jane, J. (2016). Physicochemical properties of Tibetan hull-less barley starch. *Carbohydrate Polymers*, *137*, 525–531.
- Yoshimoto, Y., Tashiro, J., Takenouchi, T., & Takeda, Y. (2000). Molecular structure and some physicochemical properties of high-amylose barley starches. *Cereal Chemistry*, *77*, 279–285.